Lyman α photolysis of solid nitromethane (CH₃NO₂) and D3-nitromethane (CD₃NO₂) – untangling the reaction mechanisms involved in the decomposition of model energetic materials

Pavlo Maksyutenko, Lloyd G. Muzangwa, Brant M. Jones and Ralf I. Kaiser*

Solid nitromethane (CH₃NO₂) along with its isotopically labelled counterpart D3-nitromethane (CD₃NO₂) ices were exposed to Lyman α photons to investigate the mechanism involved in the decomposition of energetic materials in the condensed phase. The chemical processes in the ices were monitored online and *in situ via* infrared spectroscopy complimented by temperature programmed desorption studies utilizing highly sensitive reflectron time-of-flight mass spectrometry coupled with pulsed photoionization (ReTOF-PI) at 10.49 eV. The infrared data revealed the formation of *cis*-methylnitrite (CH₃ONO), formaldehyde (H₂CO), water (H₂O), carbon monoxide (CO), and carbon dioxide (CO₂). Upon sublimation of the irradiated samples, three classes of higher molecular weight products, which are uniquely formed in the condensed phase, were identified *via* ReTOF-PI: (i) nitroso compounds [nitrosomethane (CH₃NO), nitrosoethane (C₂H₅NO), nitrosopropane (C₃H₇NO)], (ii) nitrite compounds [methylnitrite (CH₃ONO), ethylnitrite (C₂H₅ONO), propylnitrite (C₃H₇ONO)], and (iii) higher molecular weight molecules [CH₃NONOCH₃, CH₃NONO₂CH₃, CH₃OCH₂NO₂, ONCH₂CH₂NO₂]. The mechanistical information obtained in the present study suggest that the decomposition of nitromethane in the condensed phase is more complex compared to the gas phase under collision-free conditions opening up not only hitherto unobserved decomposition pathways of nitromethane (hydrogen atom loss, oxygen atom loss, retro carbene insertion), but also the blocking of several initial decomposition steps due to the 'matrix cage effect'.
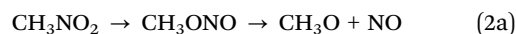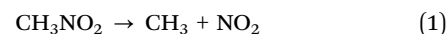
1. Introduction

Nitromethane (CH₃NO₂) is widely exploited as a prototype model compound of nitrohydrocarbon-based (RNO₂) energetic materials with a wide variety of applications. These involve the use as monopropellants,[1–3] liquid explosives,[4–9] and high-performance fuel additives for internal combustion engines as well as in pulsed detonation engines.[10] An understanding of the reaction mechanisms involved in the decomposition of nitromethane and of the successive reactions of the carbon-, nitrogen-, and oxygen-centered radical fragments produced in this process is imperative to predict the long-term stability (aging behavior),[11,12] the explosion efficiency (performance),[13,14] and the sensitivity of energetic materials to heat and shocks.[12,15–23]

Due to these implications, the decomposition mechanisms of nitromethane (CH₃NO₂) have been extensively explored under collisionless conditions in the gas phase[24–34] exploiting infrared multi photon dissociation (IRMPD) and ultraviolet

Department of Chemistry, University of Hawaii at Manoa, Honolulu, Hawaii, HI, 96822, USA. E-mail: ralfk@hawaii.edu

photodissociation (UVPD) both theoretically and experimentally for the last 30 years (Table 1, Fig. 1). These studies revealed three channels: (1) the unimolecular decomposition of nitromethane (CH₃NO₂) to the methyl radical (CH₃) and to nitrogen dioxide (NO₂)[30,35–39] *via* reaction (1) as well as (2) a roaming-mediated nitromethane (CH₃NO₂)–methylnitrite (CH₃ONO) isomerization in IRMPD studies followed by unimolecular decomposition *via* (2a) a radical pathway to the methoxy radical (CH₃O) plus nitrogen monoxide (NO) (reaction (2a) and (2b)) through a molecular elimination pathway yielding formaldehyde (H₂CO) plus nitrosylhydride (HNO) (reaction (2b)).[37–41]
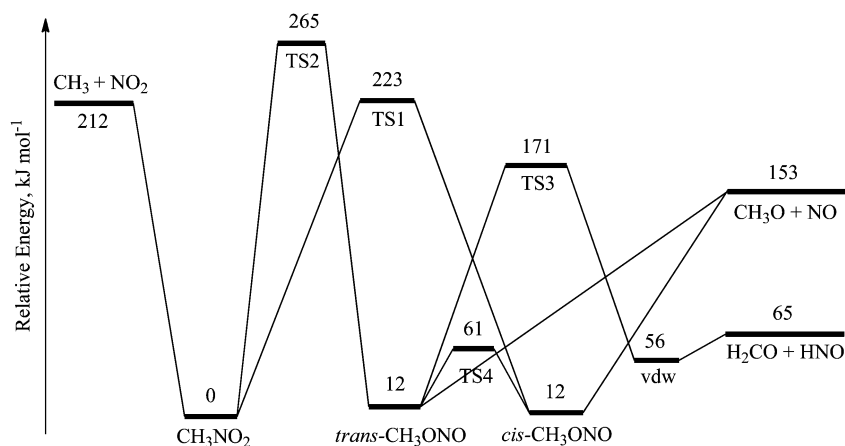
$$CH_3NO_2 \rightarrow CH_3 + NO_2 \qquad (1)$$

$$CH_3NO_2 \rightarrow CH_3ONO \rightarrow CH_3O + NO \qquad (2a)$$

$$\rightarrow H_2CO + HNO. \qquad (2b)$$

Surprisingly, in the condensed phase only a few experimental studies on the decomposition of nitromethane exist. Rebbert and Slagg (1962)[42] and Bielski *et al.* (1964)[43] conducted mercury arc photolysis of liquid nitromethane and pure nitromethane ice

7514 | *Phys. Chem. Chem. Phys.*, 2015, **17**, 7514–7527

This journal is © the Owner Societies 2015

Table 1 Compilation of results of the decomposition of nitromethane (CH_3NO_2) in the gas phase

Experimental

Authors	Method	Main results
Wodtke et al.[37]	10.6 μm IRMPD	$CH_3NO_2 + nh\nu \rightarrow CH_3 + NO_2$
		$CH_3NO_2 + nh\nu \rightarrow CH_3ONO \rightarrow CH_3O + NO$
Butler et al.[35]	194 nm UVPD ($\pi \rightarrow \pi^*$)	$CH_3NO_2 + h\nu \rightarrow CH_3 + NO_2$ (X^2A_1, A^2B_2)
Lao et al.[30]	200 and 218 nm UVPD	Electronic and vibrational predissociation pathways along the $^1B_2(\pi\pi^*)$ surface leading to NO_2 fragment
Guo et al.[36]	226 nm UVPD ($\pi \rightarrow \pi^*$)	CH_3, NO, OH, CH_3O fragments
Kohge et al.[79]	Ion imaging, 212 nm UVPD	$CH_3NO_2 + h\nu \rightarrow CH_3 + NO + O$ three-body dissociation channel
Suits et al.[40]	State selective ion imaging of NO IRMPD fragment	Roaming-mediated isomerization to CH_3ONO

Computational

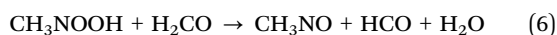| Authors	Level	Main results
Zhu and Lin[38]	Statistical calculations UCCSD(T)/CBS potential energy surface.	cis-CH_3ONO isomerization, in addition to $CH_3 + NO_2$ and trans-CH_3ONO; $CH_3O + NO$ kinetics channel dominant below 246 kJ mol^{-1} excitation.
Lin et al.[39]	Thermal decomposition kinetics.	Isomerization to CH_3ONO via a roaming TS is dominant at pressures below 2 Torr, leading to $CH_3O + NO$ and $H_2CO + HNO$. $CH_3 + NO_2$ decomposition channel becomes more important at higher pressures
Homayoon and Bowman[41]	UB3LYP/6-311+g(d,p)	Isomerization-roaming pathway to the CH_3ONO isomer and then to the $CH_3O + NO$
Suits et al.[40]	Quasi-classical trajectory calculations	Confirmed the roaming assisted isomerization pathway to $CH_3O + NO$ observed via NO ion imaging

Fig. 1 Schematic representation of the potential energy surface for the isomerization and decomposition of nitromethane (CH_3NO_2) adapted from Homayoon and Bowman.[41]

at 77 K correspondingly. These experiments suggested that the initial step of the photodissociation of nitromethane results in the formation of the methyl radical (CH_3) and to nitrogen dioxide (NO_2) in analogy to reaction (1) in the unimolecular decomposition in the gas phase. Further, broad-band photolysis of nitromethane in the range of 240 to 360 nm in an argon matrix at 20 K combined with infrared studies by Brown and Pimentel (1958)[44] and Jacox (1984)[45] proposed the formation of cis- and trans-methylnitrite (CH_3ONO). On prolonged photolysis, the absorptions of cis- and trans-methylnitrite (CH_3ONO) diminished with a growth in the absorptions of a formaldehyde (H_2CO)–nitrosylhydride (HNO)-bonded complex as well as nitrosomethanol ($ONCH_2OH$). Likewise, as the irradiation exposure continued, a water (H_2O)–isocyanic acid (HCNO) complex was monitored. Jacox suggested that the observed formation of carbon monoxide (CO) and nitrogen monoxide (NO) in the later stages of

the irradiation could be explained by the photodecomposition of (2b) reaction products; further, reaction (5) as discussed below might be responsible for the water (H_2O) production.

Very recently, Han et al.[46] and Zhang et al.[47] investigated the thermal decomposition of nitromethane (CH_3NO_2) theoretically in the condensed phase via molecular dynamics calculations at time scales of up to 200 ps. The authors predicted two initial reaction pathways: a nitromethane (CH_3NO_2) to methylnitrite (CH_3ONO) isomerization (reaction (3)) dominating at lower temperatures (2000–2500 K) and an intermolecular hydrogen atom transfer process leading to N-hydroxy-nitrosomethane (CH_3NOOH) plus a nitromethyl (CH_2NO_2) radical at elevated temperatures (3000 K) (reaction (4)). Further, hydrogen migration in nitromethane leads to aci-nitromethane ($H_2C{=}N(O)OH$), which then eliminates water (H_2O) to form isocyanic acid (HCNO) (reaction (5)). The formation of water might involve

intramolecular hydrogen atom transfers as well. Here, the hydroxyl group (OH) is predicted to originate from CH_3NOOH with the second hydrogen atom released from formaldehyde (H_2CO) leading to the formyl radical (HCO) (reaction (6)). The authors concluded that besides these low molecular weight products, the decomposition of nitromethane is anticipated to lead to larger molecules of unknown structure containing between 40% and 70% of the total carbon and nitrogen content with up to three carbon atoms per molecule.[48]

$$CH_3NO_2 \rightarrow CH_3ONO \qquad (3)$$

$$CH_3NO_2 + CH_3NO_2 \rightarrow CH_3NOOH + CH_2NO_2 \qquad (4)$$

$$CH_3NO_2 \rightarrow H_2C{=}N(O)OH \rightarrow HCNO + H_2O \qquad (5)$$

$$CH_3NOOH + H_2CO \rightarrow CH_3NO + HCO + H_2O \qquad (6)$$

Further, Reed *et al.* carried out quantum molecular dynamics calculations simulating condensed phase nitromethane (CH_3NO_2) as it undergoes chemical decomposition under explosive detonation conditions.[49,50] This study amplified the potential role of an intramolecular hydrogen atom shift from the methyl group to the oxygen atom of the nitro group forming aci-nitromethane ($H_2C{=}N(O)OH$) (reaction (5)) after about 8 ps. Close to the end of the simulation at about 100 ps, a mixture of small (stable) molecules exist such as water (H_2O), carbon dioxide (CO_2), and nitrogen (N_2). Hereafter, Guo *et al.*[47] and Citroni *et al.*[51] predicted computationally that the decomposition of nitromethane in the solid state involves two (or possibly more) molecules in the initial step leading eventually to intermolecular hydrogen atom transfer together with the generation of short-lived (picosecond) radical intermediates and the synthesis of higher-molecular weight molecules of unknown structure, which likely contain C–N–C–N-based chains. This simulation also suggested a discerning view on water molecule formation. Here, a carbon–hydrogen bond rupture in nitromethane (CH_3NO_2) leads to an energetic hydrogen atom, which is proposed to subsequently react with the NO_2 moiety of a neighboring nitromethane molecule forming a hydroxyl radical (OH) plus nitrosomethane (CH_3NO). The hydroxyl radical could eventually react with a second hydrogen atom forming a water molecule.

To summarize, the compilation of previous studies suggests that no consistent picture has emerged on the decomposition of nitromethane and the successive reactions of the carbon, nitrogen, and oxygen-bearing radical species generated in the solid state. Whereas molecular beam gas phase studies yielded valuable information on the dynamics of the decomposition of these model compounds under single collision conditions either *via* IRMPD or UVPD (reactions (1) and (2a/2b)), the decomposition of energetic materials and their model compounds in the solid state is expected to be more complex – as evident from theoretically predicted intermolecular hydrogen atom transfer, 'dimerization' reactions, and the formation of higher-molecular weight molecules of unknown structure.[46,47] This is expected to lead to a greater variety as well as more complex transient intermediates and reaction products compared to gas phase processes. Therefore, a high-level experimental investigation of

the decomposition of nitromethane in the condensed phase and the reaction of the carbon, nitrogen, and oxygen-bearing radicals generated in these processes is imperative and necessary for the future of mankind.

2. Experimental

The apparatus utilized for the present experiments has been introduced previously.[52–54] Briefly, the experiments were carried out in a contamination-free ultra-high vacuum (UHV) chamber (Fig. 2), which can be evacuated down to base pressures of a few 10^{-11} Torr with the help of two magnetically suspended turbomolecular pumps backed by an oil-free scroll pump. A cold finger assembled from oxygen free high conductivity copper (OFHC) is coupled to an UHV compatible closed-cycle helium refrigerator (Sumitomo Heavy Industries, RDK-415E). A polished silver wafer is mounted to the cold finger and pressed against a 0.1 mm thick indium foil to ensure thermal conductivity and subsequently cooling to 5.5 ± 0.1 K; the entire ensemble is freely rotatable within the horizontal center plane and translatable in the vertical (z-axis) *via* a UHV compatible bellow (McAllister, BLT106) and differentially pumped rotary feed through (Thermo-ionics Vacuum Products, RNN-600/FA/MCO). Nitromethane (CH_3NO_2, TCI AMERICA, 99+%) and D3-nitromethane (CD_3NO_2, Aldrich, 99+% D) were condensed *via* vapor deposition through a glass capillary array at a pressure of 5×10^{-8} Torr for approximately 2 minutes yielding ice sample thicknesses of 380 ± 10 nm. The thickness of the sample was determined *in situ* using He–Ne laser interferometry.[55] We derive the index of refraction by measuring the intensity ratio between maxima and minima of the measured interference curve.[56–58] From this technique, we obtain the index of refraction $n_{632nm} = 1.39 \pm 0.02$ for nitromethane ice, which is close to published data of liquid nitromethane 1.38.[59] These ices were irradiated with Lyman α vacuum ultraviolet (VUV) photons at 122 ± 5 nm for 60 hours while maintaining a constant temperature of 5.5 ± 0.1 K. Here, A 30 W deuterium lamp (McPherson Model 632) was exploited as light source. This model is coupled to an ultra-high vacuum compatible monochromator (McPherson Model 302UHV), which is equipped with a 1200 grooves per mm grating. The width of the entrance and exit slits was set to 1 mm in order to allow a sufficiently high flux of Lyman α to enter the main chamber. The ice surface was oriented normal to the incident photon beam during the irradiation with $3.5 \pm 0.5 \times 10^{12}$ photons s^{-1} cm^{-2} as determined *via* a NIST cali-brated photodiode (International Radiation Detectors Model AXUV-100G). For the on line and *in situ* identification of the newly formed molecules, a Fourier transform infrared spectro-meter (Nicolet 6700) monitored the samples throughout the duration of the experiment in the range from 6000 to 500 cm^{-1} at a resolution of 4 cm^{-1} in absorption–reflection–absorption mode. We recognize that integrated band areas can be altered by optical interference effects inherit in absorption–reflection–absorption FTIR spectroscopy as demonstrated by Teolis *et al.*;[60] however, this issue is circumvented as shown in our

7516 | *Phys. Chem. Chem. Phys.*, 2015, **17**, 7514–7527

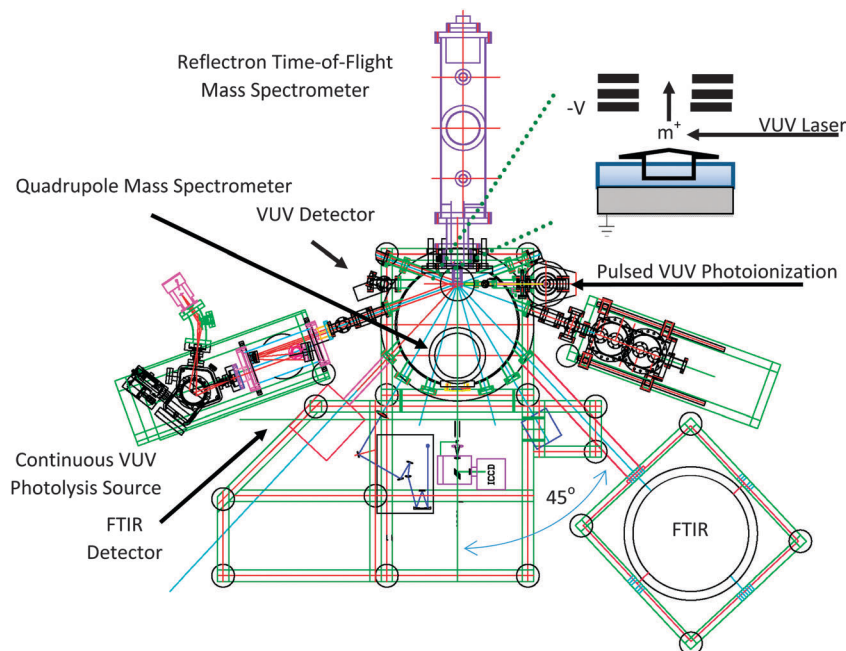This journal is © the Owner Societies 2015

Fig. 2 Schematic top view of the main chamber including the analytical instruments, Lyman α photolysis sources, photoionization laser, and the cryogenic target (point of converging lines). The inset (top right) shows the geometry of the ReTOF ion source lenses with respect to the target and ionization source. Adapted from Jones and Kaiser.[53]

group by integration of weak bands, whose absorbance remains linear with respect to the amount of ice deposited.[61]

After the irradiation, temperature programed desorption (TPD) studies were conducted by heating the irradiated ices at a rate of 0.5 K min^{-1} to 300 K. The subliming molecules were then photoionized *via* single photon ionization and detected in a reflectron time-of-flight mass spectrometer (ReTOF)[53] exploiting single photon ionization with pulsed (30 Hz) coherent vacuum ultraviolet (VUV) light at 118.2 nm (10.49 eV). Here, the third harmonic (354.6 nm) of a high-power pulsed Nd:YAG laser (Spectra Physics, PRO – 250; 30 mJ per pulse) was frequency tripled to produce the VUV photon utilizing xenon (Xe) gas as the nonlinear medium producing $3.5 \pm 0.5 \times 10^{12}$ photons cm^{-2} s^{-1} depicting a conversion efficiency of typically 10^{-4} exploiting a nonlinear four wave mixing process ($\omega_{vuv} = 3\omega_1$). A pulsed valve was housed in a doubly differentially pumped chamber held at typically 2×10^{-4} Torr when operated at 30 Hz, – 400 V, and 80 μs opening time; the pulsed valve fired 200 μs prior to the Q-switch of the Nd:YAG laser to release the xenon gas at a backing pressure of 1266 Torr (99.999%; Specialty Gases of America) in a T-shaped stainless steel adapter with 1 mm diameter hole at 25 mm in length in line with the propagating laser beam. The VUV light was then separated and directed to 1 mm above the ice surface utilizing an off-axis, differentially pumped lithium fluoride (LiF) lens, where the sublimating molecules are then photoionized. The ions were then extracted into a reflectron time-of-flight mass spectrometer whereupon the ions are mass resolved according to their arrival times. Ultimately, the ions are detected utilizing a multichannel plate with a dual chevron configuration. From here the signals were amplified using a fast pre-amplifier (Ortec 9305) and shaped with a 100 MHz discriminator.

The TOF spectra were recorded with a personal computer based multichannel scaler (FAST ComTec, P7888–1 E) using a bin width of 4 ns.

3. Results and discussion

3.1. Infrared spectroscopy

3.1.1. Qualitative analysis.
During the photolysis of nitromethane and D3-nitromethane ices with Lyman α photons, new infrared absorption features of five molecules appeared (Table 2). Compared to the neat nitromethane and D3-nitromethane ices, whose absorption features are compiled in (Table 2A), the formation of *cis*-methylnitrite (*cis*-CH$_3$ONO) – the structural isomer of nitromethane (CH$_3$NO$_2$) – was confirmed *via* its N=O stretching mode at 1615 cm^{-1} as well as its deuterated analog at 1608 cm^{-1} (Table 2B and 2C; Fig. 3A and B) in agreement with previous assignment.[62] Further, the formaldehyde molecule (H$_2$CO) was detected at 1720 cm^{-1} *via* its carbonyl stretching mode together with water/D2-water (3600–2800 cm^{-1}; 2600–2050 cm^{-1}), carbon dioxide (2343 cm^{-1}), and carbon monoxide (2137 cm^{-1}). Although searched for, we would like to stress that we did not detect any absorptions of the methyl radical (CH$_3$), nitric oxide (NO), or nitrogen dioxide (NO$_2$).

3.1.2. Quantitative analysis – reaction pathways.
Having assigned five individual molecules formed during the radiolysis of nitromethane (Table 2), we are now proposing the underlying formation pathways exploiting coupled differential equations to numerically fit the temporal profiles of the column densities of the newly formed molecules during the irradiation (Fig. 4 and 5).[63] The resulting rate constants are listed in Table 3.

This journal is © the Owner Societies 2015

Phys. Chem. Chem. Phys., 2015, **17**, 7514–7527 | 7517

Table 2 (A) Absorptions observed in nitromethane (CH_3NO_2) and D3-nitromethane (CD_3NO_2) ices. (B) New absorption features observed in the nitromethane (CH_3NO_2) ice after Lyman α photolysis. (C) New absorption features observed in the D3-nitromethane (CD_3NO_2) ice after Lyman α photolysis

(A)

This Work	Literature[80]	Assignment[80]
CH_3NO_2		
3073	3072	CH stretch (B_2)
3041	3045	CH stretch (B_1)
2963	2958	CH stretch (A_1)
1572	1571	NO stretch (B_2)
1423	1428	CH_3 bend (B_2)
1378	1381	NO stretch (A_1)
1106	1102	CH_3 rock (B_2)
663	660	NO_2 bend (A_1)
CD_3NO_2		
2281	2280	CD stretch (B_2)
1565	1567	NO stretch (B_2)
1402	1401	CD_3 bend (A_1)
1035	1038	CD_3 bend (B_2)
885	884	CD_3 rock (B_2)
632	630	NO_2 bend (A_1)

(B)

This work (cm^{-1})	Literature value (cm^{-1})	Assignment	A[81,82] ($cm\ molecule^{-1}$)
3600–2800	3500–3200[83]	H_2O (OH str.)	2.0×10^{-16}
2343	2345[45]	CO_2 (CO str.)	7.6×10^{-17}
2137	2143[45]	CO	1.1×10^{-17}
1720	1726[44]	H_2CO (CO str.)	1.8×10^{-17}
1615	1613[62]	cis-CH_3ONO (NO str.)	2.8×10^{-18}

(C)

This work (cm^{-1})	Literature value (cm^{-1})	Assignment	A[81] ($cm\ molecule^{-1}$)
2600–2050	2600–2300[84]	D_2O (OD str.)	
2343	2345[45]	CO_2 (CO str.)	7.6×10^{-17}
1608	1613[62]	cis-CD_3ONO (NO str.)	
2137	2143[45]	CO	1.1×10^{-17}

Basically these data propose that the photolysis of nitromethane initiates a branched reaction, which is followed by two sequential reaction schemes. In detail, nitromethane (CH_3NO_2) was found to isomerize first via (pseudo) first order kinetics to methylnitrite (CH_3ONO) (k_1), which then decomposes through a molecular elimination channel forming formaldehyde (H_2CO) and nitrosylhydride (HNO) (k_2).[64,65] Formaldehyde then fragments via molecular hydrogen loss forming carbon monoxide (CO) (k_3), which then reacts via atomic oxygen addition (from nitromethane) leading to carbon dioxide (CO_2) (k_4).[66,67] As proposed by Guo et al.,[47] water formation can proceed via photolysis of nitromethane forming an energetic (suprathermal) hydrogen atom, which then reacts with a second nitromethane molecule leading to the hydroxyl radical (OH), which subsequently recombined with a second hydrogen atom forming water. Note that in order to fit the formaldehyde profile, it was necessary to include a decomposition pathway from nitromethane (k_7). This pathway has never been included in any reaction scheme prior to this study and has not been identified in previous calculations (Fig. 1);

however, the non-equilibrium nature of the decomposition of nitromethane might involve higher energy isomers, which may undergo water elimination upon photolysis (Fig. 1). In particular the fast formation of water (k_5/k_6) proposed non-equilibrium chemistry and suprathermal hydrogen atoms (hydrogen atoms with an excess kinetic energy formed upon photolysis). These pathways are explored in future studies. Note that carbon dioxide can be formed by addition of suprathermal oxygen atoms to carbon monoxide; the oxygen atoms could be released via decomposition of nitromethane (CH_3NO_2) to nitrosomethane (CH_3NO) (see below).

3.1.3. Quantitative analysis – mass balance. Based on the decay profile of the nitromethane, $(2.4 \pm 0.2) \times 10^{16}$ nitromethane molecules (CH_3NO_2) were destroyed after 3.2×10^5 seconds of irradiation. This number translates into destruction rate of $(2.0 \pm 0.3) \times 10^{-2}$ molecules per photon or $(2.0 \pm 0.3) \times 10^{-3}$ molecules per absorbed eV. On the other hand, $(1.0 \pm 0.2) \times 10^{16}$ water molecules (H_2O) were produced. Smaller amounts of carbon monoxide (CO; $(1.2 \pm 0.1) \times 10^{15}$), formaldehyde ($H_2CO$; $(6.0 \pm 1.0) \times 10^{14}$), carbon dioxide ($CO_2$; $(5.0 \pm 1.0) \times 10^{14}$), and cis-methylnitrite (CH_3ONO; $(5.0 \pm 0.7) \times 10^{14}$) were also formed. Considering that two carbon monoxide molecules are needed to form one carbon dioxide molecule, these new products can account for only $55 \pm 15\%$ of the decomposing nitromethane molecules. Therefore, we have to conclude that approximately half of nitromethane molecules are transformed into newly formed products, which have remained unobserved via the infrared spectroscopic studies. Therefore, we have to apply a complementary, highly sensitive detection technique to probe these molecules upon their sublimation from the condensed phase into the gas phase: reflectron time-of-flight mass spectrometry coupled with single photon ionization.

3.2. ReTOFMS-PI

Despite the infrared data, with the exception of cis-methylnitrite (CH_3ONO), formaldehyde (H_2CO), water (H_2O), carbon monoxide (CO), and carbon dioxide (CO_2), these data alone cannot account quantitatively for the destruction of the nitromethane (CH_3NO_2) molecules. Therefore, we applied the complementary, highly sensitive ReTOFMS-PI technique to identify individual organic molecules during their sublimation events based on their mass-to-charge ratios, the sublimation temperatures, and how these mass-to-charge ratios shift upon isotope labeling. Fig. 6 depicts the ReTOFMS as a function of temperature during the warm up phase of the photolyzed nitromethane and D3-nitromethane ices. These spectra portray the intensity of the ion counts of the ionized products subliming into the gas phase at well-defined temperatures. In the nitromethane and D3-nitromethane systems, molecules with masses up to 106 amu and 112 amu, respectively, are observable. By photolyzing D3-nitromethane, we are assigning the mass-to-charge ratios via shifts in their masses upon deuteration. Further, the isotopically labeled counterparts can be identified in these ices by plotting the sublimation temperatures versus the ion counts and verifying that these species hold identical sublimation profiles (Fig. 7). The ionization
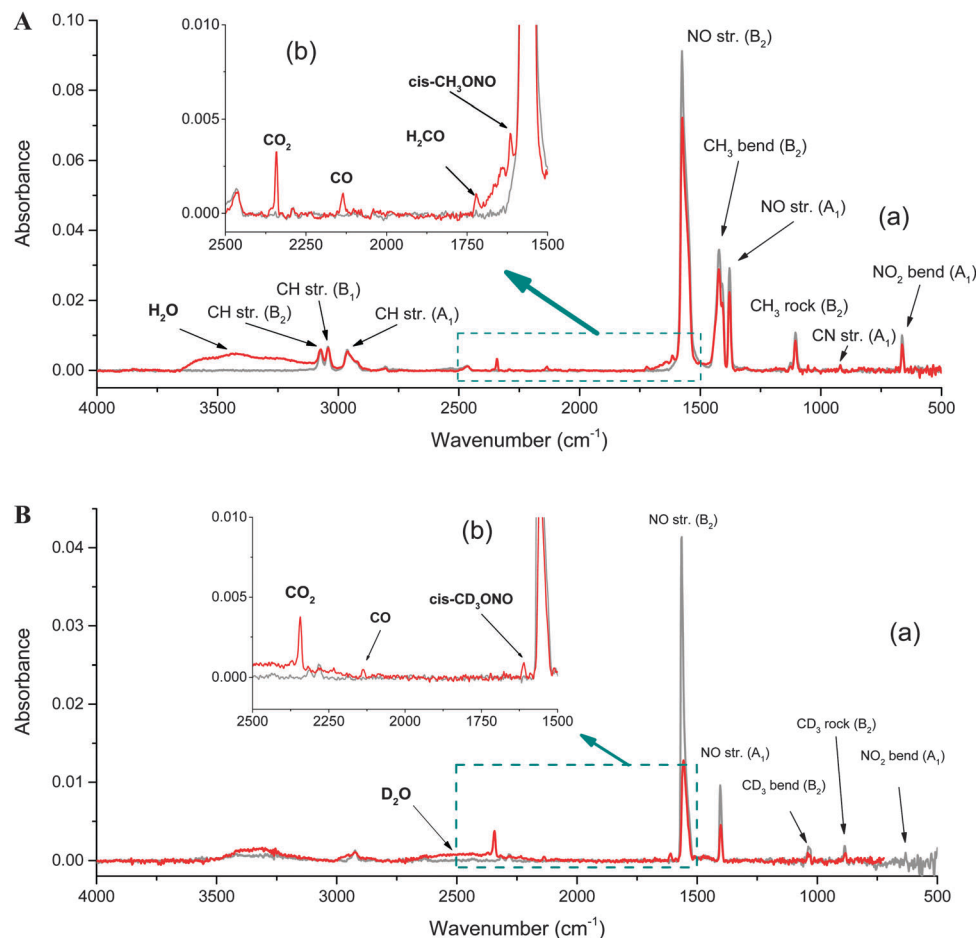
Fig. 3 (A) Infrared spectrum of the nitromethane (CH_3NO_2) ice at 5.5 K before (black) and after (red), Lyman α photolysis. (B) Infrared spectrum of the D3-nitromethane (CD_3NO_2) ice at 5.5 K before (black) and after (red), Lyman α photolysis.
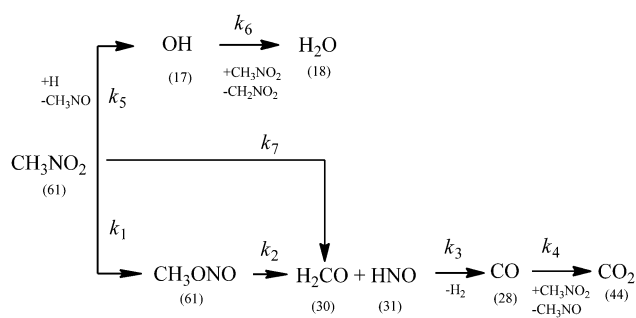

Fig. 4 Reaction scheme exploited for the kinetic fits of the temporal profiles of the newly formed molecules during nitromethane photolysis.

threshold represents another crucial factor since only species that can be ionized at a photon energy lower than 10.49 eV can be detected.

3.2.1. Lower molecular weight molecules. Let us first verify the infrared spectroscopically observed molecules. It is important to stress that the parent molecule nitromethane (CH_3NO_2; 61 amu) cannot be ionized since its ionization energy (IE) of 11.1 eV is higher than the photon energy exploited in the present studies (10.49 eV). Therefore, we recorded the sublimation profile of nitromethane and its D3-nitromethane

via traditional mass spectroscopy exploiting electron impact ionization (100 eV; 1 mA) (Fig. 8). However, its isomerization product *cis*-methylnitrite (CH_3ONO; 61 amu) together with its D3-*cis*-methylnitrite (CD_3ONO; 64 amu) counterpart as formed via reaction (3) could be easily traced via their parent ions at m/z = 61 and 64, respectively, considering their ionization energy of 10.44 eV. The TPD profiles suggest two sublimation events from about 125 K to 175 K and from 175 K to 275 K. Note that the first sublimation event correlates with the sublimation of the (D3)-nitromethane reactants (Fig. 8).

Recall that *cis*-methylnitrite can fragment via a radical (reaction (2a)) and molecular (reaction (2b)) decomposition pathway forming the methoxy radical (CH_3O; 31 amu) plus nitrogen monoxide (NO; 30 amu) and formaldehyde (H_2CO; 30 amu) plus nitrosylhydride (HNO; 31 amu). The radical decomposition pathway could be traced via nitrogen monoxide (IE = 9.26 eV), whose TPD profiles from the photolyzed nitromethane and D3-nitromethane samples are essentially identical peaking at 165 K. In contrast to the nitrogen monoxide 'free radical', the methoxy radical does not sublime but rather reacts (see below).[68,69] The molecular fragmentation channel as traced via formaldehyde (H_2CO; 30 amu) in the infrared studies can only be monitored via the molecular ion of nitrosylhydride
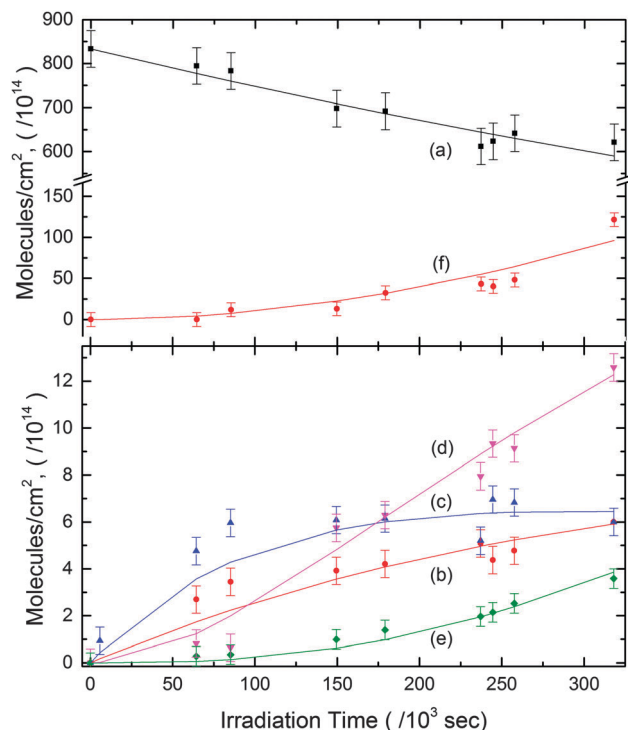
This journal is © the Owner Societies 2015

Phys. Chem. Chem. Phys., 2015, **17**, 7514–7527 | **7519**

Fig. 5 Temporal evolution of the column densities of (a) CH_3NO_2 (1402 cm^{-1} band), (b) *cis*-CH_3ONO (1615 cm^{-1} band), (c) H_2CO (1720 cm^{-1} band), (d) CO (2137 cm^{-1} band), (e) CO_2 (2343 cm^{-1} band) and (f) H_2O (3600–2800 cm^{-1} band). Kinetic fits (solid lines) have been made assuming the scheme in Fig. 4.

Table 3 Compilation of rate constants derived for the decomposition of nitromethane *via* the scheme in Fig. 4 during Lyman α exposure

	Rate constants, s^{-1}
k_1	$(3.5 \pm 0.4) \times 10^{-8}$
k_2	$(1.9 \pm 0.5) \times 10^{-6}$
k_3	$(1.0 \pm 0.2) \times 10^{-5}$
k_4	$(2.2 \pm 0.5) \times 10^{-6}$
k_5	$(1.0 \pm 0.3) \times 10^{-6}$
k_6	$(3.4 \pm 1.5) \times 10^{-6}$
k_7	$(9.2 \pm 1.5) \times 10^{-8}$

(HNO; 31 amu) and D1-nitrosylhydride (DNO; 32 amu) holding an ionization energy of 10.1 eV, since formaldehyde (IE = 10.9 eV) cannot be ionized under our experimental conditions. It is important to stress that nitrogen monoxide (NO; 30 amu) can also react with hydrogen atoms in the sample (H; 1 amu) to form nitrosylhydride (HNO; 31 amu) as well. Both nitrosylhydride (HNO) and D1-nitrosylhydride (DNO) sublime together with the (D3) nitromethane reactants. It is important to highlight that the ionization energies of carbon monoxide (CO; 28 amu; IE = 14.0 eV) and carbon dioxide (CO_2; 44 amu; IE = 13.8 eV) are too high to be observed *via* RETOF-PI.

Finally, signal at m/z = 45 could be attributed to nitrosomethane (CH_3NO; 45 amu; IE = 9.3 eV) likely formed *via* atomic oxygen loss photodissociation of nitromethane (CH_3NO_2; 61 amu); this process is highly endoergic by 363 kJ mol^{-1}. The formation of nitrosomethane can be verified based on the TPD profiled of the D3-nitromethane sample at m/z = 48 *via* the

molecular ion peak of D3-nitrosomethane (CD_3NO; 48 amu); both TPD profiles at m/z = 45 and 48 for the photolyzed nitromethane and D3-nitromethane sample match exceptionally well depicting two distinct sublimation events prior to the sublimation of the nitromethane reactant molecules (90–130 K) and during the sublimation of the nitromethane reactants (140–175 K), as well as sublimation of a higher mass in the 250 to 300 K range producing CH_3NO fragments. The central peak could also borrow intensity from m/z = 75 product ($CH_3CH_2NO_2$) fragmentation.

3.2.2. Higher molecular weight molecules derived from carbene reactions. A detailed analysis of the TPD profiles and the mass-to-charge ratios of the ionized products reveals patterns of a molecular mass growth by 14 amu (nitromethane sample) and 16 amu (D3-nitromethane sample), which could be reflected in a mass growth through reaction of precursor molecules with carbene (CH_2) and D2-carbene (CD_2), respectively. This growth process by 14 amu and 16 amu is evident from signal detected at mass-to-charge ratios of 45 *versus* 59 and 61 *versus* 75 from the photolyzed nitromethane samples, which is also matched at mass-to-charge ratios of 48 *versus* 64 and 64 *versus* 80 in the photolyzed D3-nitromethane ices. Carbene – if it is in its singlet state – can insert without barrier[70] into the carbon–hydrogen bond of the methyl group of nitrosomethane (CH_3NO; 45 amu) forming nitrosoethane (CH_3CH_2NO; 59 amu; IE = 10.1 eV). In the D3-nitromethane system, this shifts from D3-nitrosomethane (CD_3NO; 48 amu) to D5-nitrosoethane (CD_3CD_2NO; 64 amu), *i.e.* a mass difference of 5 amu as reflected by the presence of five deuterium atoms instead of hydrogen. Likewise, singlet carbene can also insert into the carbon–hydrogen bond of methylnitrite (CH_3ONO; 61 amu) forming ethylnitrite (CH_3CH_2ONO; 75 amu); this mechanism is also verified in the D3-nitromethane system *via* the observation of D3-methylnitrite (CD_3ONO; 64 amu) and D5-ethylnitrite (CD_3CD_2ONO; 80 amu) formed *via* D2-carbene insertion. Note that the ionization energy of ethylnitrite of 10.53 eV is slightly above the photon energy of 10.49 eV; however as demonstrated earlier in our group, the electric fields of the repeller plate can lower the ionization energy (Stark effect) by at least 0.04 eV.[53] Note that ethylnitrite (CH_3CH_2ONO; 75 amu) can also be formed *via* carbene insertion into a carbon–hydrogen bond of nitromethane forming nitroethane ($CH_3CH_2NO_2$) followed by nitro–nitrito isomerization to ethylnitrite (CH_3CH_2ONO; 75 amu). However, the ionization energy of nitroethane ($CH_3CH_2NO_2$) of 10.9 eV is too high compared to the 10.49 eV of the photon exploited in the current experiments. It should be stressed that the TPD profiles of 59 and 64 ((D5)nitrosoethane) as well as 75 and 80 ((D5)ethylnitrite) match nicely thus highlighting the importance of deuterium substitution in the assignment of potential reaction products.

The assignment of the weak signal at m/z = 89 could be explained by a successive mass growth *via* a second carbene insertion – this time upon reaction with nitroethane ($CH_3CH_2NO_2$; 75 amu) or ethylnitrite (CH_3CH_2ONO; 75 amu) – forming nitro(iso)propane ($C_3H_7NO_2$; 89 amu) or (iso)propylnitrite (C_3H_7ONO; 89 amu). Here, only propylnitrite (IE = 10.34 eV) and isopropylnitrite (IE = 10.23 eV) can be photoionizaed, but not nitropropane (IE = 10.78 eV) or isonitropropane (IE = 10.74 eV).
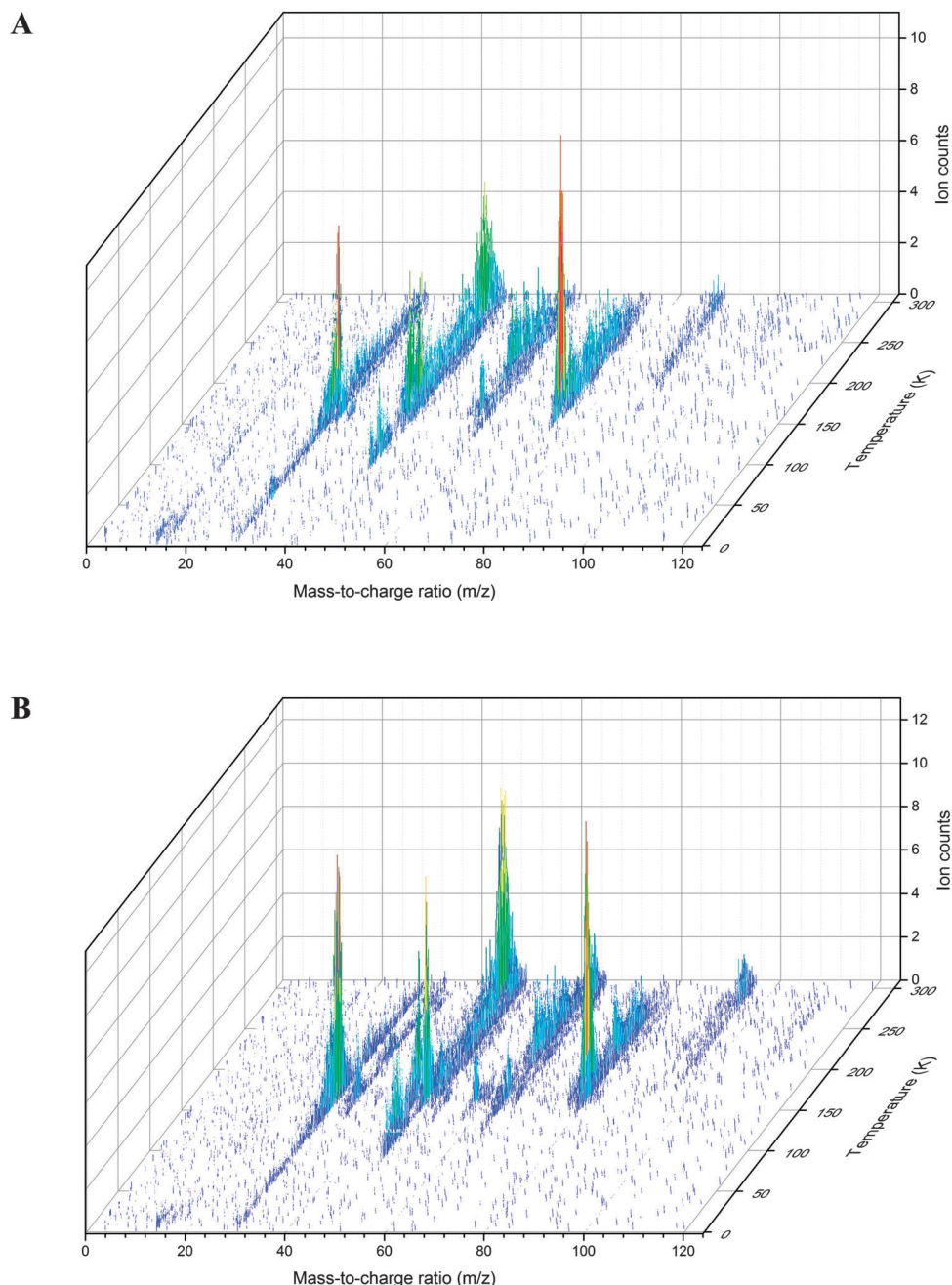
7520 | *Phys. Chem. Chem. Phys.*, 2015, **17**, 7514–7527

This journal is © the Owner Societies 2015

Fig. 6 (A) ReTOFMS-PI data as a function of temperature of the products subliming into the gas phase from photolyzed nitromethane (CH_3NO_2). (B) ReTOFMS-PI data as a function of temperature of the products subliming into the gas phase from photolyzed D3-nitromethane (CD_3NO_2).

Note that the corresponding signal in the D3-nitromethane system at $m/z = 96$ is too high to account only for the formation of D7-(iso)propylnitrite, and a hitherto unidentified product has to contribute to this signal as well. Likewise, the weak signal at $m/z = 73$ could origin from a successive mass growth *via* a second carbene insertion – this time upon reaction with nitrosoethane (CH_3CH_2NO; 59 amu) forming nitroso(iso)-propane (C_3H_7NO; 73 amu). However, the corresponding signal in the D3-nitromethane system at $m/z = 80$ is dominated by the formation of D5-ethylnitrite (CD_3CD_2ONO; 80 amu), and a definite assignment is not feasible at the present stage. It is worth mentioning that signal at $m/z = 73$ could also be explained *via* molecular hydrogen elimination from ethylnitrite (CH_3CH_2ONO; 75 amu) forming vinylnitrite (C_2H_3ONO; 73 amu). The ionization energy of the nitroethylene isomer ($C_2H_3NO_2$; 73 amu) of 11.0 eV is too high to be ionized under the present experimental conditions. A hydrogen elimination in nitroso-methane (CH_3CH_2NO; 59 amu) could account for signal at $m/z = 57$ (nitrosoethylene; 57 amu) matched by signal at $m/z = 60$ (D3-nitrosoethylene; 60 amu) in the photolyzed D3-nitromethane sample. Finally, we would like to address a potential pathway to form singlet carbene. Previous experiments investigating the
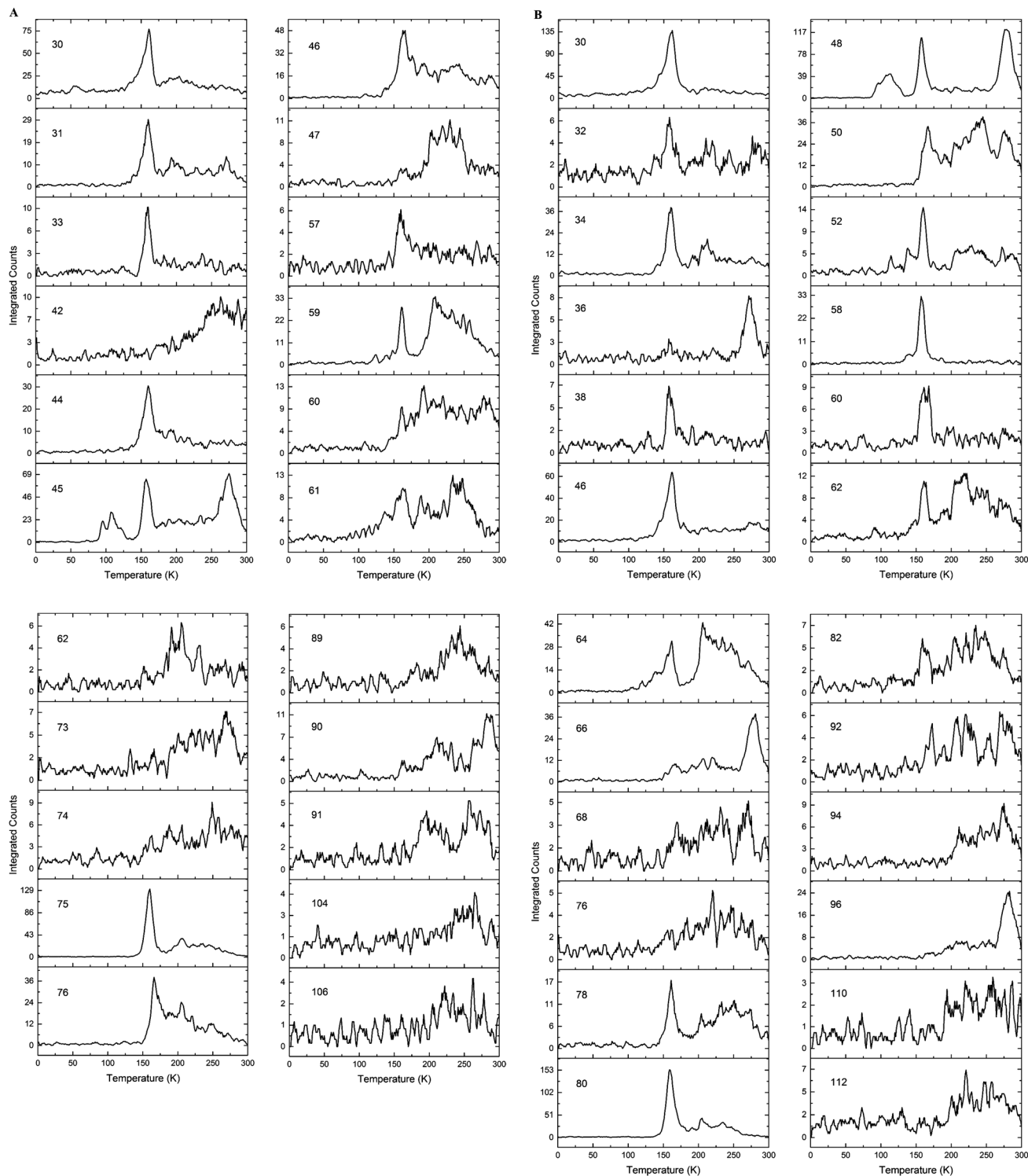
Fig. 7 (A) Temperature programmed desorption profiles of products formed in Lyman α irradiated nitromethane (CH_3NO_2). Mass-to-charge ratios of the sublimating products are indicated in the top left corner of each graph. (B) Temperature programmed desorption profiles of products formed in Lyman α irradiated D3-nitromethane (CD_3NO_2). Mass-to-charge ratios of the sublimating products are indicated in the top left corner of each graph.

interaction of ionizing radiation with cryogenic films of methanol (CH_3OH),[52] methylamine (CH_3NH_2),[71] and ethane (CH_3CH_3)[72] provided compelling evidence on the formation of methane (CH_4) formed *via* retro-insertion of singlet oxygen atoms (O),

singlet nitrene (NH), and singlet carbene (CH_2). If this mechanism also holds for nitromethane, retroinsertion of singlet carbene should yield nitrous acid (HONO; 47 amu), whose ionization energy (IE = 11.3 eV) is above the 10.49 eV photon exploited in the present
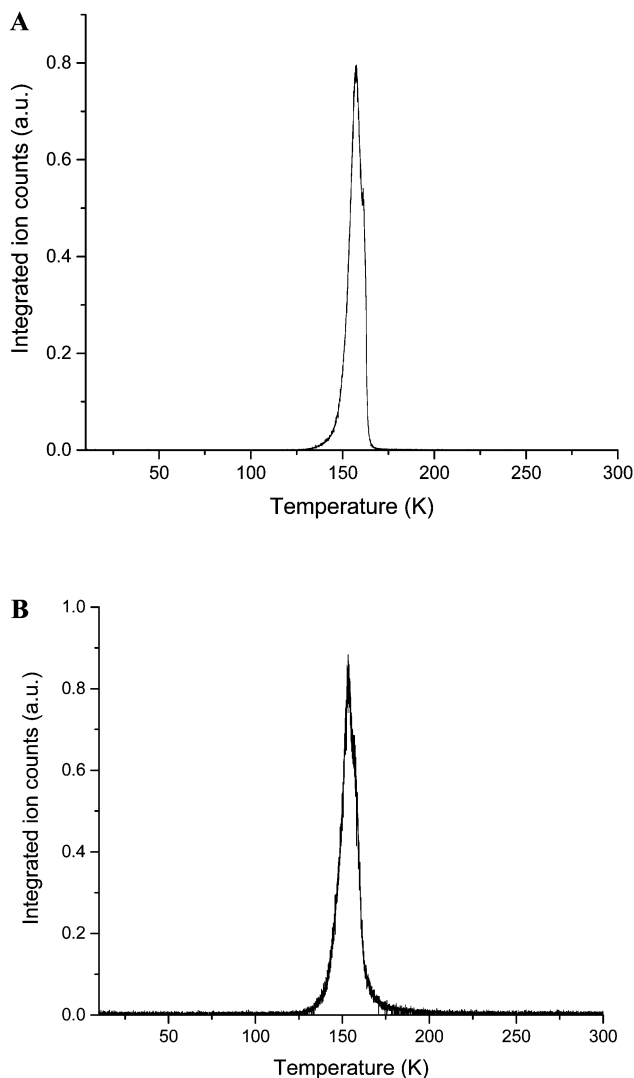
A

B

Fig. 8 (A) Temperature programmed desorption profile of Lyman α irradiated nitromethane detected by a quadruple mass spectrometer *via* electron impact ionization at *m/z* = 61 amu (CH₃NO₂). (B) Temperature programmed desorption profile of Lyman α irradiated D3-nitromethane detected by a quadruple mass spectrometer *via* electron impact ionization at *m/z* = 64 amu (CD₃NO₂).

experiments. This process requires 415 kJ mol^{-1}, which can be covered by the 10.2 eV of the Lyman α photon.

It is important to note that in principle, a series of hydrogen abstractions or losses followed by methyl loss could present a viable alternative. However, we do not detect any methyl radical, which is easily traceable *via* its 608 cm^{-1} mode as verified in our group in irradiated methane samples at 10 K. Additional experiments will be conducted in forthcoming studies involving mixtures of D3 and H3 nitromethane and methylnitrite ices to elucidate the involvement of potential minor methyl group pathways.

3.2.3. Higher molecular weight molecules derived from addition reactions. The initial step of the formation of the molecules with the chemical formulae CH_5NO (47 amu) and $CH_4N_2O_2$ (76 amu) could be the addition of suprathermal

hydrogen atoms to the oxygen atom of the nitrogen–oxygen double bound in nitrosomethane (CH_3NO; 45 amu) forming a CH_3NOH (46 amu) transient radical. Typically addition of hydrogen atoms to closed shell molecules carrying double bonds have entrance barriers of 10 to 30 kJ mol^{-1};[73,74] therefore, this process requires suprathermal hydrogen atoms holding excess kinetic energy to pass the entrance barrier to reaction. The CH_3NOH radical (46 amu) can then react with a second hydrogen atom (1 amu) or with nitrogen monoxide (30 amu) without entrance barrier *via* radical–radical reactions to form the observed *N*-methylhydroxylamine (CH_3NHOH; 47 amu; IE = 9.0–9.8 eV) and *N*-nitroso-*N*-methylhydroxylamine (CH_3N-(NO)OH; 76 amu). Note that the ionization energy of the latter is unknown, but should fall below the ionization energy of hydroxylamine (NH_2OH; IE = 9.6–10.0 eV). The formation of *N*-methylhydroxylamine (CH_3NHOH; 47 amu) is also verified *via* its D5-counterpart (CDH_3NDOD; 52 amu) in the D3-nitro methane photolyzed sample *via* the sublimation event from 170 K to 250 K. Finally, *N*-nitroso-*N*-methylhydroxylamine ($CH_3N(NO)OH$; 76 amu) can be matched with the sublimation events peaking at 160 K and 210 K in the D3-nitromethane photolyzed sample *via* m/z = 80 ($CD_3N(NO)OD$). It should be noted, however, that the dominating fraction of signal at m/z = 80 originates from ethylnitrite (CH_3CH_2ONO).

3.2.4. Higher molecular weight molecules derived from two nitromethane units. We also observed higher molecular masses from 90 amu to 106 amu, which can be explained through the involvement (including their respective fragments) of two building blocks of nitromethane molecules. First, both nitromethane (CH_3NO_2; 61 amu) and nitrosomethane (CH_3NO; 45 amu) can lose a hydrogen atom forming the nitromethyl (CH_2NO_2; 60 amu) and nitrosomethyl (CH_2NO; 44 amu) upon exposure to Lyman α photons. These processes are strongly endoergic by 439 kJ mol^{-1} and 245 kJ mol^{-1}, which can be overcome by the 10.49 eV Lyman α photon. Both radicals can now recombine forming a molecule of the chemical formula $C_2H_4N_2O_3$. Based on a simple radical–radical recombination, the product should be 1-nitroso-2-nitroethane ($ONCH_2CH_2NO_2$; 104 amu). Based on the TPD profile, the ion counts are very small, but well above background level. Nevertheless, due to the lack of signal in the D3-nitromethane system at m/z = 108, this assignment has to be confirmed in future studies. The known structures of the chemical formula $C_2H_4N_2O_3$ include methasonic acid ($HONCHCH_2NO_2$) and ethylnitrolic acid ($CH_3C(NOH)NO_2$), although the poor stability of the former makes it a less likely candidate.[75] Further, we monitored a small signal at m/z = 91, which possibly can be connected to the radical–radical reaction of the nitromethyl radical (CH_2NO_2; 60 amu) with the methoxy radical (CH_3O; 31 amu) forming methoxynitromethanol ($CH_3OCH_2NO_2$; 91 amu). The sublimation event from 175 K to 220 K in the D3-nitromethane system at m/z = 96 amu ($CD_3OCD_2NO_2$) could support this assignment.

Finally, we monitored signal at m/z = 90 and 106. Formally, this can be attributed to dimers of nitrosomethane, *i.e.* (CH_3NO–CH_3NO; 90 amu; IE = 8.6 eV), and of reaction products of nitrosomethane (CH_3NO; 45 amu) with nitromethane

(CH$_3$NO$_2$; 61 amu) forming CH$_3$NO–CH$_3$NO$_2$ (106 amu). Nitrosomethane (CH$_3$NO) is known to react rapidly *via* dimerization in the gas phase forming (*E*)-azodioxymethane;[76] this dimerization could also be triggered in the condensed phase *via* Lyman α photons forming a nitrogen–nitrogen double bond in the nitrosomethane dimer. It is important to note that the TPD profile at *m/z* = 90 suggests two sublimation events at 175 to 250 K and 250 K to 300 K. The sublimation event at 250 K to 300 K is also matched at *m/z* = 45, *i.e.* the nitrosomethane monomer. This pattern suggests that upon photoionization at 10.49 eV, the cation also undergoes dissociation to form a singly ionized nitrosomethane monomer giving rise to signal at *m/z* = 45. Note that a comparison of the data in the D3-nitromethane system at *m/z* = 96 shifts the mass-to-charge by 6 amu; this verifies the presence of six hydrogen/deuterium atoms in the molecules at 90 amu (nitromethane system) and 96 amu (D3-nitromethane system) as evident from similar sublimation profiles from 250 K to 300 K. Having assigned the signal at *m/z* = 90 to the nitrosomethane dimer, we are now analyzing the signal at *m/z* = 106 – the highest observed mass-to-charge ratio as formally derived from reaction of a nitrosomethane (CH$_3$NO; 45 amu) with nitromethane (CH$_3$NO$_2$; 61 amu) yielding CH$_3$NO–CH$_3$NO$_2$ (106 amu). Here, the TPD profiles of the nitromethane and D-nitromethane systems at *m/z* = 106 and *m/z* = 112 correlate nicely in particular from 200 K to 300 K suggesting that this molecule – of hitherto unknown structure – contains six hydrogen/deuterium atoms. Citroni *et al.*[51] computationally described the formation of C$_2$H$_6$N$_2$O$_3$ isomers. According to the simulation of nitromethane decomposition under high pressure, the molecule was formed *via* nitrosomethyl radical (CH$_2$NO) reaction with CH$_3$NOOH.

3.2.5. Remaining TPD profiles. We are finally discussing the remaining TPD profiles with decreasing *m/z* values, which cannot be grouped in any of the previous categories. First, signal at *m/z* = 91 might be attributed to 1-hydroxy-2-ethanenitrite (HOCH$_2$CH$_2$ONO; 91 amu), which could be formally derived *via* oxygen atom insertion into a carbon–hydrogen bond of ethylnitrite (CH$_3$CH$_2$ONO). Signal at *m/z* = 62 might origin from dimethylperoxide (CH$_3$OOCH$_3$; 62 amu; IE = 9.7 eV) possibly synthesized *via* recombination of two methoxy (CH$_3$O) radicals. Based on the TPD profiles, signal at *m/z* = 60 (CH$_2$NO$_2$$^+$) likely originates as a fragment from *m/z* = 104 (ONCH$_2$CH$_2$NO$_2$$^+$), while *m/z* = 44 (CH$_2NO^+$) might be a fragment ion from *m/z* = 45 nitrosomethane (CH$_3$NO); we do not observe carbon dioxide (CO$_2$; IE = 13.8 eV) or dinitrogen monoxide (N$_2$O; IE = 12.9 eV). Finally, signal at *m/z* = 46 could be attributed to nitrogen dioxide (NO$_2$; 46 amu; IE = 9.6 eV). Recall that the photodissociation of nitromethane into methyl radicals and nitrogen dioxide represents the dominating process in the gas phase photolysis under collisionless conditions; however, we were unable to observe even traces of nitrogen dioxide or methyl radicals – or their reaction products – *via* infrared spectroscopy or ReTOF, respectively. Therefore, in the present experiments, nitrogen dioxide might be formed *via* reactions of oxygen atoms with nitrogen monoxide rather than *via* photodissociation of nitromethane.

4. Summary and conclusions

The present study examined experimentally the response of thin films of nitromethane and D3-nitromethane upon photolysis with Lyman α photons (10.2 eV) at 5.5 K and probed the newly formed molecules *via* two complementary techniques: FTIR and ReTOFMS-PI. Our FTIR data revealed the formation of *cis*-methylnitrite (CH$_3$ONO), formaldehyde (H$_2$CO), water (H$_2$O), carbon monoxide (CO), and carbon dioxide (CO$_2$). The fits of the temporal evolution of these absorptions indicate that the isomerization of nitromethane (CH$_3$NO$_2$) to methylnitrite (CH$_3$ONO) formed *via* (pseudo) first order kinetics followed by a molecular decomposition pathway forming formaldehyde (H$_2$CO) and nitrosylhydride (HNO) presents a key reaction pathway in the condensed phase; we were unable to spectroscopically detect any products of the radical decomposition pathway, *i.e.* the methoxy radical (CH$_3$O) and nitrogen monoxide (NO); likewise the radical decomposition pathway to form the methyl radical (CH$_3$) plus nitrogen dioxide (NO$_2$) is absent. This is in strong contrast to previous gas phase IRMPD studies under collisionless conditions revealing that both radical and the molecular decomposition pathways are open. Note that in the condensed phase (ice), the 'matrix cage effect' facilitates a recombination of the formed radicals. In the gas phase, the initially formed fragments fly undisturbed to the detector; this is hindered in the solid state since the surrounding nitromethane matrix limits the radical fragments from leaving the formation site. If the methoxy radical and nitrogen monoxide are formed initially upon Lyman α exposure, they can recombine in the matrix cage to 'reform' nitromethane. Likewise, upon decomposition of nitromethane, the methyl radical (CH$_3$) and the nitrogen dioxide fragments (NO$_2$) can recombine. However, this recombination can happen *via* formation of a carbon–nitrogen bond *via* a barrier-less reaction of the methyl radical with the radical center located at the nitrogen atom of nitrogen dioxide (NO$_2$) yielding again nitromethane or through recombination with the radical center located – in a resonance structure – at the oxygen atom of nitrogen dioxide (NO$_2$) forming methylnitrite (CH$_3$ONO). The latter reaction pathway can be considered the condensed phase analogy of the roaming reaction mechanism in the gas phase.[39,41,77,78] Consequently, both roaming (gas phase) and matrix cage (condensed phase) result *de facto* in the formation of methylnitrite (CH$_3$ONO). Note that the recombination of two closed shell molecules – formaldehyde (H$_2$CO) and nitrosylhydride (HNO) formed in the molecular decomposition pathway involves a significant entrance barrier of at least 110 kJ mol^{-1} (Fig. 1). Therefore, once formed and thermalized at 5.5 K, formaldehyde and nitrosylhydride cannot react back to methylnitrite (CH$_3$ONO) without absorbing a photon since the reversed reaction is blocked by the entrance barrier. Based on the infrared data, it is crucial to point out that only 55 ± 15% of the destroyed nitromethane molecules have been accounted for to be incorporated into *cis*-methylnitrite (CH$_3$ONO), formaldehyde (H$_2$CO), water (H$_2$O), carbon monoxide (CO), and carbon dioxide (CO$_2$). Recall that previous molecular dynamics calculations

7524 | *Phys. Chem. Chem. Phys.*, 2015, **17**, 7514–7527

This journal is © the Owner Societies 2015

on the thermal decomposition of nitromethane (CH_3NO_2) in the condensed phase proposed that between 40% and 70% of the total carbon and nitrogen content are incorporated into newly formed molecules carrying up to three carbon atoms per molecule. Therefore, the infrared studied verify that 45% $\pm$ 15% of the molecules have been converted to higher molecular weight product, which cannot be formed under collisionless conditions in the gas phase.

The higher molecular weight products, *which are unique to the condensed phase*, have been monitored *via* ReTOFMS-PI. We identified three major product classes (Fig. 9, Table 4) containing molecules with up to three carbon atoms, which formally require up to three nitromethane 'building blocks': (i) nitroso compounds, (ii) nitrite compounds, and (iii) higher molecular weight molecules – among them formal dimerization products. *First*, we observed molecular growth processes, which can be rationalized *via* successive insertion of carbene (CH_2) into carbon–hydrogen bonds yielding from nitrosomethane (CH_3NO) a series of *nitrosoalkanes*: nitrosoethane (C_2H_5NO) and nitrosopropane (C_3H_7NO). Likewise – with the beginning of methylnitrite (CH_3ONO), the carbene insertions lead to the formation a series of *nitritoalkanes*: ethylnitrite (C_2H_5ONO) and propylnitrite (C_3H_7ONO). Both C_2H_3NO and C_2H_3ONO can be formed *via* molecular hydrogen loss from their nitrosomethane (C_2H_5NO) and ethylnitrite (C_2H_5ONO) precursors. *Second*, we detected four molecules, which formally require the reaction of

(fragments of) two nitromethane building blocks: $CH_3NONOCH_3$, $CH_3NONO_2CH_3$, and tentatively due to the limited signal-to-noise $CH_3OCH_2NO_2$ and $ONCH_2CH_2NO_2$. Here, the synthesis of $CH_3NONOCH_3$ as well as $CH_3NONO_2CH_3$ requires the reaction of two neighboring nitrosomethane and nitrosomethane/nitromethane molecules – reaction pathways which have been predicted based on quantum molecular dynamics calculations.[51] *Finally*, the pathways to methylhydroxyamine (CH_3NHOH) and nitrosomethylhydroxylamine ($CH_3N(NO)OH$) require the presence of suprathermal hydrogen atoms, which react first with nitrosomethane (CH_3NO) to form the CH_3NOH transient radical, which then reacts with a hydrogen atom and nitrogen monoxide molecule, respectively. The formation path to 1-nitroso-2-nitroethane ($ONCH_2CH_2NO_2$) requires the recombination of the nitrosomethyl (CH_2NO) and nitromethyl (CH_2NO_2) radicals, which in turn are generated *via* photolysis of nitrosomethane (CH_3NO) and nitromethane (CH_3NO_2), respectively, in overall endoergic reactions of typically 440 kJ mol^{-1}.

Finally, with respect to the understanding of the decomposition of model compounds of energetic materials, it is important to highlight novel reaction mechanisms on the decomposition of nitromethane (pathways (7) to (9)), which have not been observed in previous gas phase IRMPD and UVPD experiments. These are the decomposition of nitromethane to the nitromethyl radical (CH_2NO_2) plus suprathermal atomic hydrogen (H), which has excess energies of up to 5.8 eV
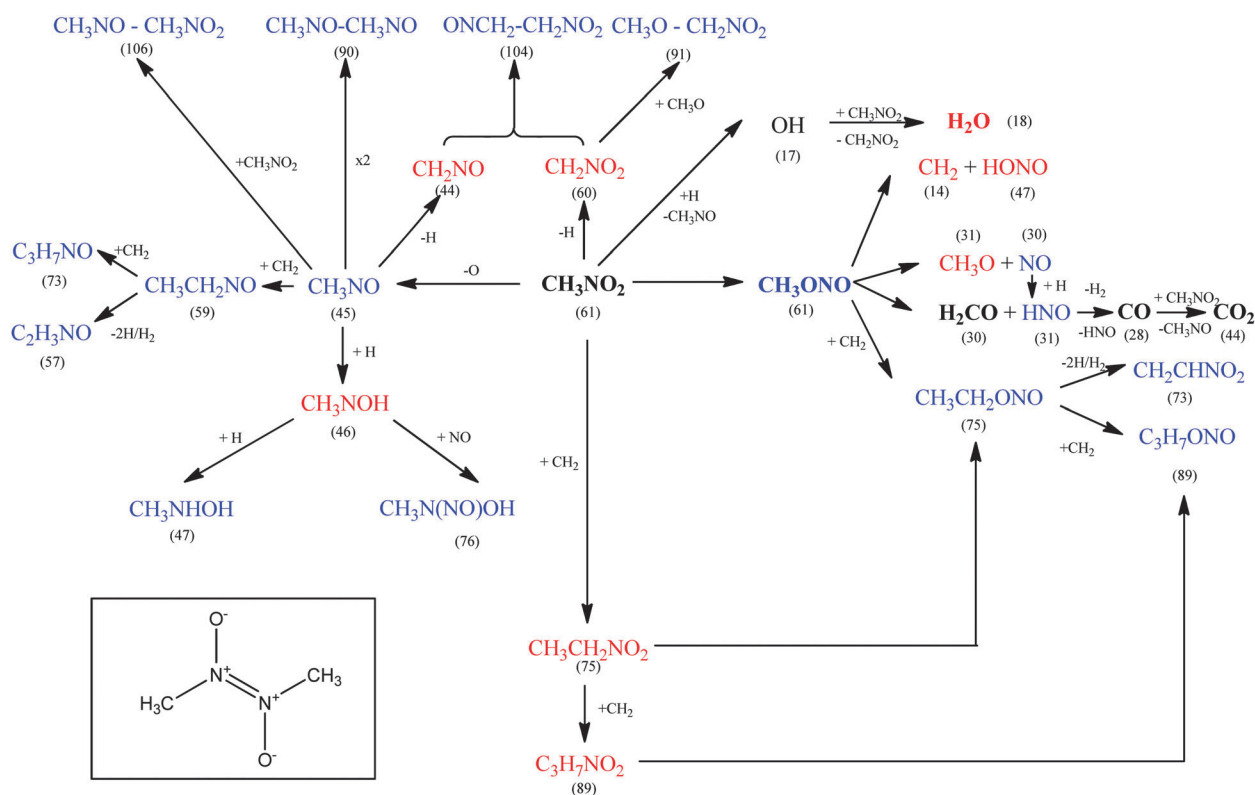
Fig. 9 Compiled reaction mechanisms taking place in nitromethane (CH_3NO_2) ice film under Lyman α irradiation. Bold: infrared detection; blue: ReTOF detection; red: inferred reaction intermediates. The boxed structure represents the molecular structure of the 'nitrosomethane dimer' (90 amu), which can exist in its *cis* and/or *trans* form.

This journal is © the Owner Societies 2015

Phys. Chem. Chem. Phys., 2015, **17**, 7514–7527 | **7525**

Table 4 Compilation of product classes formed in the photolysis of nitromethane by Lyman α. Compounds in italics are identified tentatively. Molecular weights of the products are given in parenthesis; values in italics are for the fully deuterated products formed in the D3-nitromethane system

Nitroso compounds	Nitrite compounds
CH_3NO (45 amu; *48 amu*)	CH_3ONO (61 amu; *64 amu*)
C_2H_5NO (59 amu; *64 amu*) C_2H_3NO (57 amu; *60 amu*)	C_2H_5ONO (75 amu; *80 amu*) C_2H_3ONO (73 amu; *76 amu*)
C_3H_7NO (73 amu; *80 amu*)	C_3H_7ONO (89 amu; *96 amu*)

Complex products
$CH_3NONOCH_3$ (90 amu; *96 amu*)
$CH_3NONO_2CH_3$ (106 amu; *112 amu*)
CH_3NHOH (47 amu; *52 amu*)
$CH_3N(NO)OH$ (76 amu; *80 amu*)
$CH_3OCH_2NO_2$ (91 amu; 96 amu)
$ONCH_2CH_2NO_2$ (104 amu; 108 amu)

Open shell reaction intermediates
H, O, CH_2, CH_3O, NO, NO_2

(reaction (7)), to nitrosomethane (CH_3NO) plus atomic oxygen (O) (reaction (8)), and to singlet carbene (CH_2) plus nitrous acid (HONO) (reaction (9)).

$$CH_3NO_2 + h\nu \rightarrow CH_2NO_2 + H \quad \Delta_R G = +439 \text{ kJ mol}^{-1} \quad (7)$$

$$CH_3NO_2 + h\nu \rightarrow CH_3NO + O \quad \Delta_R G = +363 \text{ kJ mol}^{-1} \quad (8)$$

$$CH_3NO_2 + h\nu \rightarrow CH_2 + HONO \quad \Delta_R G = +415 \text{ kJ mol}^{-1} \quad (9)$$

These processes form distinct carbon-centered radicals upon Lyman α photolysis, which can react with neighboring closed shall molecules and/or radicals yielding distinct product classes, which are not accessible in classical gas phase IRMPD and UVPD experiments under collisionless conditions (nitroso compounds, nitrite compounds, higher molecular weight molecules). Future experiments will exploit a newly built pulsed coherent VUV light source (4 eV to 13 eV) utilizing resonance-enhanced nonlinear four wave mixing to photoionize the subliming molecules at different wavelengths. This will aid in the identification of additional, specific isomers – among them higher energy isomers of nitromethane – based upon their distinctive ionization energies to eventually provide a comprehensive inventory, which molecules can be formed in the decomposition of nitromethane in the condensed phase.

Acknowledgements

References

1 S. Kelzenberg, N. Eisenreich, W. Eckl and V. Weiser, *Propellants, Explos., Pyrotech.*, 1999, **24**, 189–194.

2 E. Boyer and K. K. Kuo, *Proc. Combust. Inst.*, 2007, **31**, 2045–2053.

3 U. Schaller, V. Weiser, J. Hurttlen, T. Keiher and H. Krause, Presented in part at the Fraunhofer-Institut für Chemische Technologie (International Annual Conference) #44, 2013.

4 Y. X. Zhang and S. H. Bauer, *J. Phys. Chem. B*, 1997, **101**, 8717–8726.

5 J. M. Winey and Y. M. Gupta, *J. Phys. Chem. B*, 1997, **101**, 10733–10743.

6 J. M. Winey and Y. M. Gupta, *J. Phys. Chem. A*, 1997, **101**, 9333–9340.

7 V. Bouyer, I. Darbord, P. Herve, G. Baudin, C. Le Gallic, F. Clement and G. Chavent, *Combust. Flame*, 2006, **144**, 139–150.

8 M. Genetier, A. Osmont and G. Baudin, *J. Phys.: Conf. Ser.*, 2014, **500**, 192001.

9 M. R. Armstrong, J. M. Zaug, C. D. Grant, J. C. Crowhurst and S. Bastea, *J. Phys. Chem. A*, 2014, **118**, 6148–6153.

10 Q. Zhang, W. Li, D. C. Lin, N. He and Y. Duan, *J. Hazard. Mater.*, 2011, **185**, 756–762.

11 L. E. Fried, M. R. Manaa and J. P. Lewis, *Adv. Ser. Phys. Chem.*, 2005, **16**, 275.

12 J. C. Oxley, *Theor. Comput. Chem.*, 2003, **12**, 5.

13 R. P. Singh, R. D. Verma, D. T. Meshri and J. M. Shreeve, *Angew. Chem., Int. Ed.*, 2006, **45**, 3584–3601.

14 G. D. Kozak, *Propellants, Explos., Pyrotech.*, 2005, **30**, 291–297.

15 G. F. Adams and R. W. Shaw, *Annu. Rev. Phys. Chem.*, 1992, **43**, 311–340.

16 B. Vogelsanger and B. Berger, Presented in part at the Int. Annu. Conf. ICT, 2005.

17 The NATO munitions safety information analysis centre (MSIAC).

18 E. Deschambault, D. Watt, F. Peugeot and P. Touze, Presented in part at the Int. Annu. Conf. ICT, 2006.

19 A. K. Sikder and N. Sikder, *J. Hazard. Mater.*, 2004, **112**, 1–15.

20 D. M. Badgujar, M. B. Talawar, S. N. Asthana and P. P. Mahulikar, *J. Hazard. Mater.*, 2008, **151**, 289–305.

21 W. d. Klerk, G. R. Brouwer and H. Keizers, Presented in part at the Int. Annu. Conf. ITC, 2006.

22 A. Bhattacharya, Y. Q. Guo and E. R. Bernstein, *Acc. Chem. Res.*, 2010, **43**, 1476–1485.

23 T. B. Brill and K. J. James, *Chem. Rev.*, 1993, **93**, 2667–2692.

24 T. Nagata, M. Suzuki, K. Suzuki, T. Kondow and K. Kuchitsu, *Chem. Phys.*, 1984, **88**, 163–170.

7526 | *Phys. Chem. Chem. Phys.*, 2015, **17**, 7514–7527

This journal is © the Owner Societies 2015

25 I. M. Napier and R. G. W. Norrish, *Proc. R. Soc. A*, 1966, **299**, 317.

26 E. Hirschlaff and R. G. W. Norrish, *J. Chem. Soc.*, 1936, 1580.

27 B. E. Rockney and E. R. Grant, *J. Chem. Phys.*, 1983, **79**, 708.

28 A. M. Renlund and W. M. Trott, *Chem. Phys. Lett.*, 1984, **107**, 555–560.

29 J. C. Mialocq and J. C. Stephenson, *Chem. Phys.*, 1986, **106**, 281–291.

30 K. Q. Lao, E. Jensen, P. W. Kash and L. J. Butler, *J. Chem. Phys.*, 1990, **93**, 3958–3969.

31 D. B. Moss, K. A. Trentelman and P. L. Houston, *J. Chem. Phys.*, 1992, **96**, 237–247.

32 J. B. Simeonsson, G. W. Lemire and R. C. Sausa, *Anal. Chem.*, 1994, **66**, 2272–2278.

33 K. W. D. Ledingham, C. Kosmidis, S. Georgiou, S. Couris and R. P. Singhal, *Chem. Phys. Lett.*, 1995, **247**, 555–563.

34 G. D. Greenblatt, H. Zuckermann and Y. Haas, *Chem. Phys. Lett.*, 1987, **134**, 593–599.

35 L. J. Butler, D. Krajnovich, Y. T. Lee, G. Ondrey and R. Bersohn, *J. Chem. Phys.*, 1983, **79**, 1708–1722.

36 Y. Q. Guo, A. Bhattacharya and E. R. Bernstein, *J. Phys. Chem. A*, 2009, **113**, 85–96.

37 A. M. Wodtke, E. J. Hintsa and Y. T. Lee, *J. Chem. Phys.*, 1986, **84**, 1044–1045.

38 R. S. Zhu and M. C. Lin, *Chem. Phys. Lett.*, 2009, **478**, 11–16.

39 R. S. Zhu, P. Raghunath and M. C. Lin, *J. Phys. Chem. A*, 2013, **117**, 7308–7313.

40 A. Dey, R. Fernando, C. Abeysekera, Z. Homayoon, J. M. Bowman and A. G. Suits, *J. Chem. Phys.*, 2014, **140**, 054305.

41 Z. Homayoon and J. M. Bowman, *J. Phys. Chem. A*, 2013, **117**, 11665–11672.

42 R. Rebbert and N. Slagg, *Bull. Soc. Chim. Belg.*, 1962, **71**, 709–721.

43 B. H. J. Bielski and R. B. Timmons, *J. Phys. Chem.*, 1964, **68**, 347–352.

44 H. W. Brown and G. C. Pimentel, *J. Chem. Phys.*, 1958, **29**, 883–888.

45 M. E. Jacox, *J. Phys. Chem.*, 1984, **88**, 3373–3379.

46 S.-p. Han, A. C. van Duin, W. A. Goddard III and A. Strachan, *J. Phys. Chem. B*, 2011, **115**, 6534–6540.

47 F. Guo, X.-l. Cheng and H. Zhang, *J. Phys. Chem. A*, 2012, **116**, 3514–3520.

48 C. M. Tarver, *AIP Conf. Proc.*, 2006, **845**, 1026–1029.

49 L. A. Pellouchoud and E. J. Reed, *J. Phys. Chem. A*, 2013, **117**, 12288–12298.

50 E. J. Reed, M. Riad Manaa, L. E. Fried, K. R. Glaesemann and J. D. Joannopoulos, *Nat. Phys.*, 2008, **4**, 72–76.

51 M. Citroni, R. Bini, M. Pagliai, G. Cardini and V. Schettino, *J. Phys. Chem. B*, 2010, **114**, 9420–9428.

52 S. Maity, R. I. Kaiser and B. M. Jones, *Faraday Discuss.*, 2014, **168**, 485–516.

53 B. M. Jones and R. I. Kaiser, *J. Phys. Chem. Lett.*, 2013, **4**, 1965–1971.

54 C. J. Bennett, S. J. Brotton, B. M. Jones, A. K. Misra, S. K. Sharma and R. I. Kaiser, *Anal. Chem.*, 2013, **85**, 5659–5665.

55 A. S. Heavens, *Optical Properties of Thin Solid Films*, Butterworths Scientific Publications, London, 1955.

56 P. Winsemius, F. F. v. Kampen, H. P. Lengkeek and C. G. v. Went, *J. Phys. F: Met. Phys.*, 1976, **6**, 1583.

57 A. M. Goodman, *Appl. Opt.*, 1978, **17**, 2779–2787.

58 M. S. Westley, G. A. Baratta and R. A. Baragiola, *J. Chem. Phys.*, 1998, **108**, 3321–3326.

59 NIST Chemistry WebBook.

60 B. D. Teolis, M. J. Loeffler, U. Raut, M. Famá and R. A. Baragiola, *Icarus*, 2007, **190**, 274–279.

61 K. I. Öberg, R. T. Garrod, E. F. van Dishoeck and H. Linnartz, *Astron. Astrophys.*, 2009, **504**, 891–913.

62 M. Bodenbinder, S. E. Ulic and H. Willner, *J. Phys. Chem.*, 1994, **98**, 6441–6444.

63 M. Frenklach, H. Wang and M. J. Roabinowitch, *Prog. Energy Combust. Sci.*, 1992, **19**, 47.

64 M. E. Jacox and F. L. Rook, *J. Phys. Chem.*, 1982, **86**, 2899–2904.

65 R. Müller, P. Russegger and J. R. Huber, *Chem. Phys.*, 1982, **70**, 281–290.

66 C. S. Jamieson, A. M. Mebel and R. I. Kaiser, *Astrophys. J., Suppl. Ser.*, 2006, **163**, 184.

67 C. J. Bennett, C. S. Jamieson and R. I. Kaiser, *Phys. Chem. Chem. Phys.*, 2009, **11**, 4210–4218.

68 C. J. Bennett, S.-H. Chen, B.-J. Sun, A. H. Chang and R. I. Kaiser, *Astrophys. J.*, 2007, **660**, 1588.

69 S. Maity, R. I. Kaiser and B. M. Jones, *Faraday Discuss.*, 2014, **168**, 485–516.

70 R. D. Bach, M. D. Su, E. Aldabbagh, J. L. Andres and H. B. Schlegel, *J. Am. Chem. Soc.*, 1993, **115**, 10237–10246.

71 P. D. Holtom, C. J. Bennett, Y. Osamura, N. J. Mason and R. I. Kaiser, *Astrophys. J.*, 2005, **626**, 940.

72 Y. Kim, C. Bennett, L.-H. Chen, K. O'Brien and R. Kaiser, *Astrophys. J.*, 2010, **711**, 744.

73 W. L. Hase, H. B. Schlegel, V. Balbyshev and M. Page, *J. Phys. Chem.*, 1996, **100**, 5354–5361.

74 C. Sosa and H. Bernhard Schlegel, *Int. J. Quantum Chem.*, 1986, **29**, 1001–1015.

75 D. Morgan, *J. Org. Chem.*, 1962, **27**, 4646–4649.

76 F. Thomassy and F. Lampe, *J. Phys. Chem.*, 1970, **74**, 1188–1193.

77 J. M. Bowman and B. C. Shepler, *Annu. Rev. Phys. Chem.*, 2011, **62**, 531–553.

78 K. Prozument, Y. V. Suleimanov, B. Buesser, J. M. Oldham, W. H. Green, A. G. Suits and R. W. Field, *J. Phys. Chem. Lett.*, 2014, **5**, 3641–3648.

79 Y. Kohge, T. Hanada, M. Sumida, K. Yamasaki and H. Kohguchi, *Chem. Phys. Lett.*, 2013, **556**, 49–54.

80 F. D. Verderame, J. A. Lannon, L. E. Harris, W. G. Thomas and E. A. Lucia, *J. Chem. Phys.*, 1972, **56**, 2638–2647.

81 P. A. Gerakines, *Astron. Astrophys.*, 1995, **296**, 810–818.

82 J. B. Chris, C. Shih-Hua, S. Bing-Jian, H. H. C. Agnes and I. K. Ralf, *Astrophys. J.*, 2007, **660**, 1588.

83 U. Raut, M. Loeffler, R. Vidal and R. Baragiola, 35th Lunar and Planetary Science Conference, League City, Texas, March 15–19, 2004, abstract no. 1922.

84 W. Zheng, D. Jewitt and R. I. Kaiser, *Chem. Phys. Lett.*, 2007, **435**, 289–294.

This journal is © the Owner Societies 2015

Phys. Chem. Chem. Phys., 2015, **17**, 7514–7527 | 7527